Theoretical Study and Rate Constant Calculation of the Cl + HOCl and H + HOCl Reactions

Li Wang, Jing-yao Liu, Ze-sheng Li,* Xu-ri Huang, and Chia-chung Sun

Institute of Theoretical Chemistry, State Key Laboratory of Theoretical and Computational Chemistry, Jilin University, Changchun 130023, P. R. China

Received: December 17, 2002; In Final Form: April 3, 2003

The present calculations represent the first theoretical study of the mechanism of the reactions Cl + HOCl → products (R1) and H + HOCl → products (R2). A direct dynamics method is employed to perform the dynamics calculations of the two reactions. Optimized geometries and frequencies of all of the stationary points and extra points along the minimum-energy path (MEP) are obtained at the MP2/6-311+G(2d, 2p) level of theory. For the system of HOCl with Cl atoms, two complexes with energies less than that of the reactants are located in the reactant channel of the Cl abstraction and H abstraction. The energy profiles of two the reactions are refined with the interpolated single-point energy (ISPE) method at the G3//MP2 level. The rate constants are evaluated using the improved canonical variational transition-state theory (ICVT) with a small-curvature tunneling correction (SCT) over a range of temperatures from 220−2000 K. Agreement between the ICVT/SCT rate constants and the experimental values is good. Our calculations show that in the low-temperature range the branching ratio to the hydrogen abstraction channel for the two reactions is negligible, and the reactions proceed practically via chlorine abstraction, leading to the formation of OH + Cl_2 and OH + HCl, respectively; for the reaction Cl + HOCl, the hydrogen-abstraction channel appears to be probable as the temperature increases. Furthermore, the calculated rate constants are also consistent with the study of the reverse reaction OH + Cl_2 → Cl + HOCl. The tunneling correction has an important contribution in the calculation of rate constants in the low-temperature range.

Introduction

Hypochlorous acid (HOCl) is known to play a crucial role in the atmospheric chemistry of halogen oxide radicals and in ozone layer depletion.[1] The use of HOCl began to attract attention in 1976 when an atmospheric modeling study suggested that HOCl could serve as a temporary reservoir for active chlorine atoms in the stratosphere.[2] Although photochemical removal is considered to be its major removal process, the reaction of HOCl with atmospheric radical species is of interest for modeling purpose.[3−7] A few experimental kinetic studies have been performed on the reaction of HOCl with Cl atoms at 298 K[4−6] and in the temperature range from 243−365 K.[3] From a mechanistic point of view, two reaction pathways are available:

$$\mathrm{Cl + HOCl \rightarrow HCl + ClO} \quad (1a)$$

$$\rightarrow \mathrm{Cl_2 + OH} \quad (1b)$$

There is a significant discrepancy in the reported values of the product branching ratios. The results obtained from Ennis et al.[5] and Kukui et al.[6] showed that the reaction of Cl + HOCl proceeds predominantly via the Cl-abstraction channel (1b) with branching ratios of $k_{1b}/k = (0.91 \pm 0.06)$ and (0.96 ± 0.05), respectively, which are at variance with the value of (0.24 ± 0.11) determined by Vogt et al..[4] The total rate−temperature expression of $k = (3.0 \pm 0.5) \times 10^{-12} \exp[-(130 \pm 60)/T]$ cm^3 $molecule^{-1}$ s^{-1} was presented by Cook et al.[3] over the temperature range from 243−365 K. For the H + HOCl reaction, two kinetic studies were undertaken at 298 K with two kinds of proposed reverse viewpoints on the mechanism (i.e., the abstraction of the hydrogen[4] or the abstraction of the chloride[7] as the major product channel):

$$\mathrm{H + HOCl \rightarrow H_2 + ClO} \quad (2a)$$

$$\rightarrow \mathrm{HCl + OH} \quad (2b)$$

Thus, to gain deep insight into the reaction mechanism of above two reactions, further theoretical studies are very desirable. To the best of our knowledge, little theoretical attention has been paid to the reactions of HOCl with Cl and H atoms.

Here, a dual-level approach (X//Y)[8−10] is employed to study the kinetic nature of the reactions. In this methodology, information on the potential energy surface (PES) is obtained directly from ab initio electronic structure calculations. It is found that a reactant complex with energy slightly less than that of the reactant is located in the reactant channel of reactions 1a and 1b. Subsequently, by means of the Polyrate 8.4.1 program,[11] the rate constants are calculated using the variational transition-state theory (VTST)[12−14] proposed by Truhlar and coworkers for each reaction channel of the two reactions as well as the reverse reaction of 1b, Cl_2 + OH → HOCl + Cl. The specific form of VTST that we used is the improved canonical variational transition-state theory (ICVT)[15] with the small-curvature tunneling (SCT)[16,17] method. The comparison between theoretical and experimental results is discussed.

Calculation Methods

The ab initio calculations are carried out by the Gaussian 98 program.[18] The geometries and frequencies of all of the stationary points including reactants, complexes (C1 and C2), transition states (TSs), and products involved in two reactions

* Corresponding author. E-mail: liujy121@163.com, ljy121@mail.jlu.edu.cn. Fax: +86-431-8945942.

10.1021/jp0277558 CCC: $25.00
Published on Web 05/28/2003

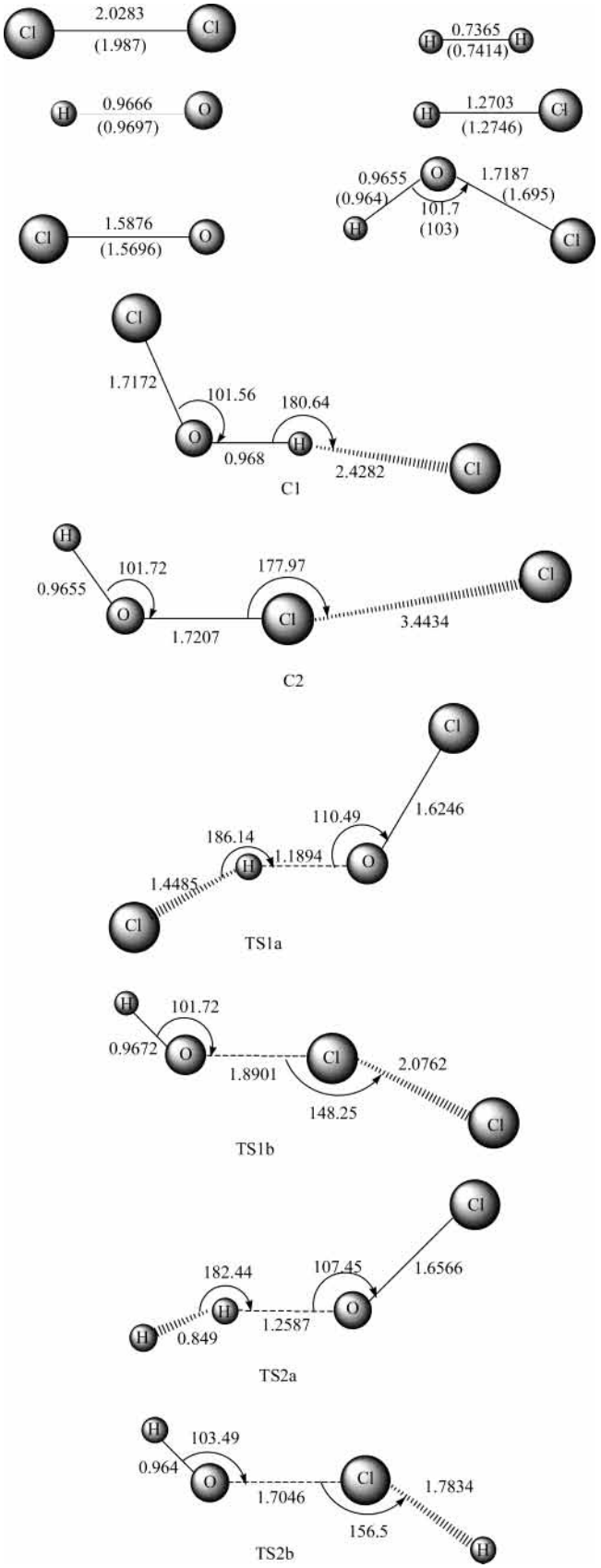

Figure 1. Optimized geometries of HOCl, C1, C2, Cl_2, OH, H_2, HCl, ClO, and four transition states at the MP2/6-311+G(2d, 2p) level. The values in the parentheses are the experimental values.[23−25] Bond lengths are in angstroms, and angles are in degrees.

are optimized by using restricted or unrestricted second-order Møller−Plesset perturbation theory with the 6-311+G(2d, 2p) basis set (MP2/6-311+G(2d, 2p)). To obtain more reliable reaction energies and barrier heights, single-point calculations for the stationary points are carried out at the G3 level of theory[19] using the MP2-optimized geometries. The minimum-energy path (MEP) is calculated by the intrinsic reaction coordinate (IRC) theory with a gradient step size of 0.05 (amu)$^{1/2}$ bohr at the MP2 level to confirm that the TS really connects with minima along the reaction path. Also, first and second energy derivatives at geometries along the MEP are obtained to calculate the curvature of the reaction path and to calculate the generalized vibrational frequencies along the reaction path. The dual-level potential profile along the reaction path is further refined with the interpolated single-point energy (ISPE) method,[20] in which a few extra single-point calculations are needed to correct the lower-level reaction path.

TABLE 1: Calculated and Experimental Frequencies (cm^{-1}) of the Reactants and Products at the MP2/6-311+G(2d, 2p) Level

	MP2/6-311+G(2d, 2p)	exptl
HOCl	729, 1267, 3804	724, 1239, 3609[a]
ClO	809	854[b]
Cl_2	560	560[c]
HCl	3002	2991[c]
OH	3818	3738[c]
H_2	4529	4401[c]
C1	37, 104, 240, 732,1299,3753	
C2	37, 49, 51, 725, 1264, 3804	
TS1a	3452i, 157, 569, 815, 917,1280	
TS1b	627i, 206, 357, 542, 980, 3799	
TS2a	2547i, 383, 670,858,1029,2066	
TS2b	1207i, 273, 417,983,1244,3823	

[a] From ref 26. [b] From ref 24. [c] From ref 25.

On the basis of initial information, the rate constant for each reaction channel is calculated by using the improved canonical variational transition (ICVT)[15] theory with the small-curvature tunneling (SCT)[16,17] approximation. Because the harmonic frequencies for the internal rotation in the two transition states for the Cl + HOCl reaction are found to be low, whereas for the H + HOCl reaction they are rather high, in the present study, all vibrations are treated in the harmonic oscillator approximation for the H + HOCl reaction; for the reaction Cl + HOCl, except for the lowest vibrational mode that is treated using the hindered rotor model,[21] all other vibrational modes are treated as separable harmonic oscillators. The partition function of the lowest vibrational mode is evaluated using the hindered partition function expressions of Truhlar and Chuang.[21,22] The $^2P_{3/2}$ and $^2P_{1/2}$ electronic states of the Cl atom, with an 881-cm^{-1} splitting due to spin−orbit coupling, are used in the calculation of the electronic partition functions. In addition, for the reverse reaction 1b, Cl_2 + OH → HOCl + Cl, we also include the two electronic states for the OH radical, with a 140-cm^{-1} splitting in the $^2\Pi$ ground state, in calculating its electronic partition functions. The curvature components are calculated by using a quadratic fit to obtain the derivative of the gradient with respect to the reaction coordinate. Finally, the total rate constant is obtained from the sum of the individual rate constant.

Results and Discussion

1. Stationary Points. The geometric parameters of all of the reactants, complexes (C1 and C2 located at the reactant side), transition states, and products optimized at the MP2/6-311+G(2d, 2p) level are given in Figure 1 together with the available experimental values.[23−25] The geometries of the reactants and products agree with the experimental values to within 2.08%. In complexes C1 and C2, the H−Cl and Cl−Cl

TABLE 2: Enthalpies (kcal mol^{-1}) at the MP2/6-311+G(2d, 2p) and G3//MP2 Levels and Available Experimental Values

levels	HOCl + Cl → HCl + ClO	HOCl + Cl → Cl_2 + OH	HOCl + H → H_2 + ClO	HOCl + H → HCl + OH
MP2/6-311+G(2d, 2p)	2.06	2.48	4.06	−45.66
G3//MP2	−7.67	−1.75	−9.03	−47.78
exptl[a]	−9.07	−1.87	−10.12	−47.09

[a] From ref 25.

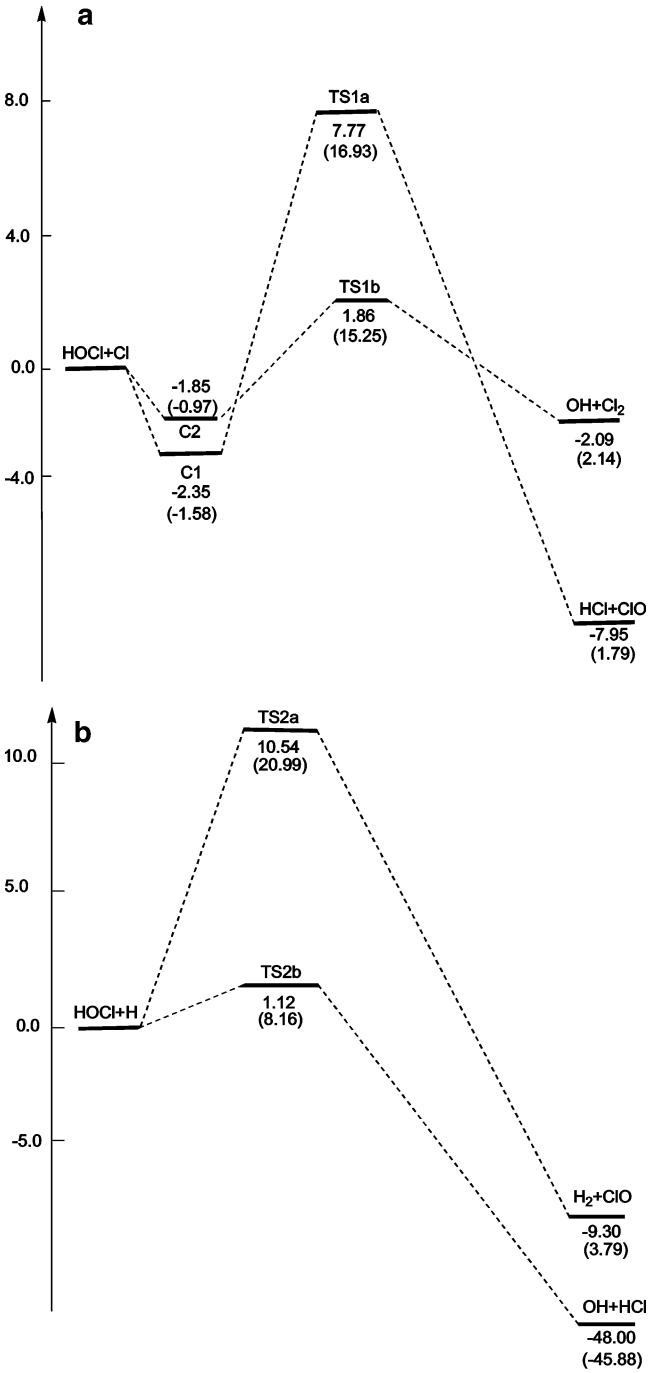

Figure 2. Schematic pathways for the reactions (a) Cl + HOCl and (b) H + HOCl. Relative energies with ZPE at the G3//MP2/6-311+G(2d, 2p) level are in kcal mol^{-1}. The values in parentheses are those obtained at the MP2/6-311+G(2d, 2p) level.

bond distances are 2.428 and 3.443 Å, respectively, and other bond distances (H−O and O−Cl) are similar to those of the reactant (HOCl). In TS1a, TS1b, and TS2a structures, the breaking bonds H−O and Cl−O increase by 23, 10, and 30%, respectively, compared to the H−O and Cl−O equilibrium bond lengths in isolated HOCl, and the forming bonds H−Cl, Cl−Cl, and H−H are elongated by 14, 2.4, and 15% with respect to the equilibrium bond lengths of the molecules HCl, Cl_2, and H_2, respectively. The elongation of the breaking bond is greater than that of the forming bond, indicating that TS1a, TS1b, and TS2a are productlike (i.e., the reactions will proceed via late transition states). However, the geometry of TS2b is much closer to the reactant structure, and H-abstraction reaction 2b will proceed via an early transition state.

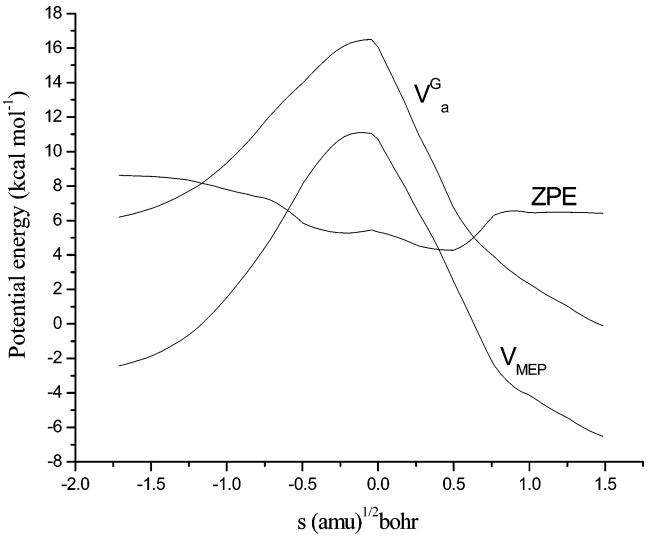

Figure 3. Classical potential energy curve (V_{MEP}), ground-state vibrationally adiabatic energy curve (V_a^G), and zero-point energy curve (ZPE) as functions of s (amu)$^{1/2}$ bohr at the G3//MP2/6-311+G(2d, 2p) level for Cl + HOCl → HCl + ClO.

The harmonic vibrational frequencies are calculated at the same level of theory to characterize the nature of each critical point and to make zero-point energy (ZPE) corrections. The number of imaginary frequencies (0 or 1) indicates whether a minimum or a transition state has been located. The harmonic vibrational frequencies of all of the stationary points along with the available experimental data[24−26] are shown in Table 1. Most of our calculated frequencies are in good agreement with the experimental values, with the largest deviation within 5.4%. Two complexes, which are located in the reactant channels of reaction R1a and R1b, correspond to all real frequencies. The transition state is identified with only one negative eigenvalue of the Hessian matrix. The imaginary frequencies of four TSs are 3452i, 627i, 2547i, and 1207i cm^{-1}, respectively.

The reaction enthalpies (ΔH°_{298}) of the Cl + HOCl and H + HOCl reactions are listed in Table 2. The MP2 calculations estimate that reactions 1a, 1b, and 2a are endothermic by 2.06, 2.48, and 4.06 kcal mol^{-1}, respectively, and these reactions are exothermic at the G3//MP2/6-311+G(2d, 2p) level. The calculated ΔH°_{298} results of −7.67, −1.75, −9.03, and −47.78 kcal mol^{-1} for the four reactions are in good agreement with the corresponding experimental values of −9.07, −1.87, −10.12, and −47.09 kcal mol^{-1}, respectively, which are derived from the experimental standard heats of formation[25] (Cl, 29.02 kcal mol^{-1}; Cl_2, 0 kcal mol^{-1}; HOCl, −17.82 kcal mol^{-1}; OH, 9.33 kcal mol^{-1}; HCl, −22.08 kcal mol^{-1}; ClO, 24.22 kcal mol^{-1}; H, 52.15 kcal mol^{-1}; H_2, 0 kcal mol^{-1}). Note that the spin

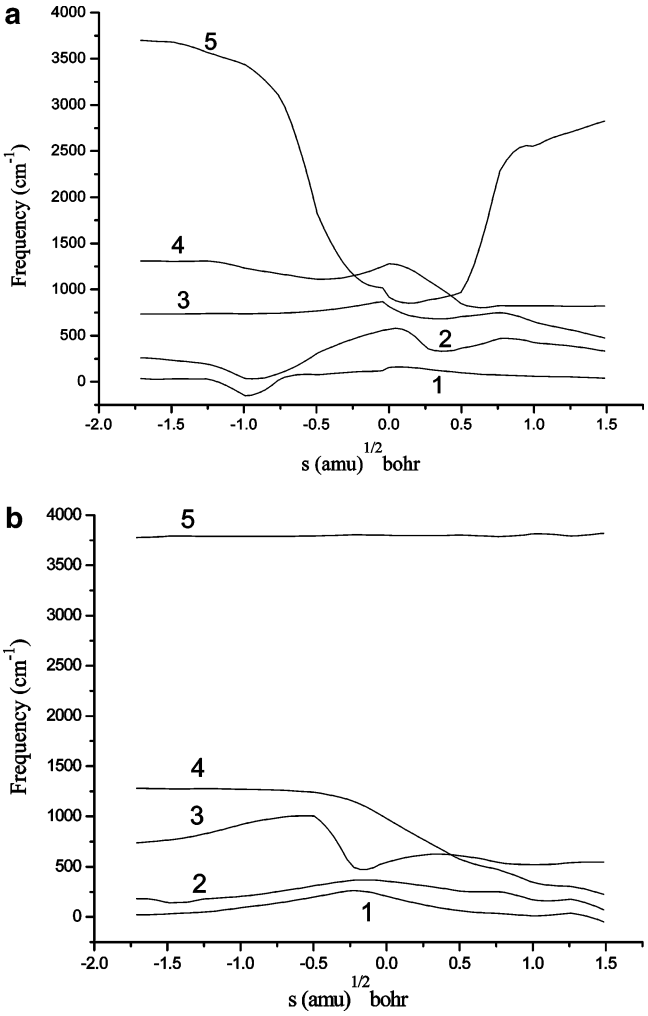

Figure 4. Changes in the generalized normal-mode vibrational frequencies as function of s (amu)$^{1/2}$ bohr at the MP2/6-311+G(2d, 2p) level for **(a)** Cl + HOCl → HCl + ClO and **(b)** Cl + HOCl → Cl_2 + OH.

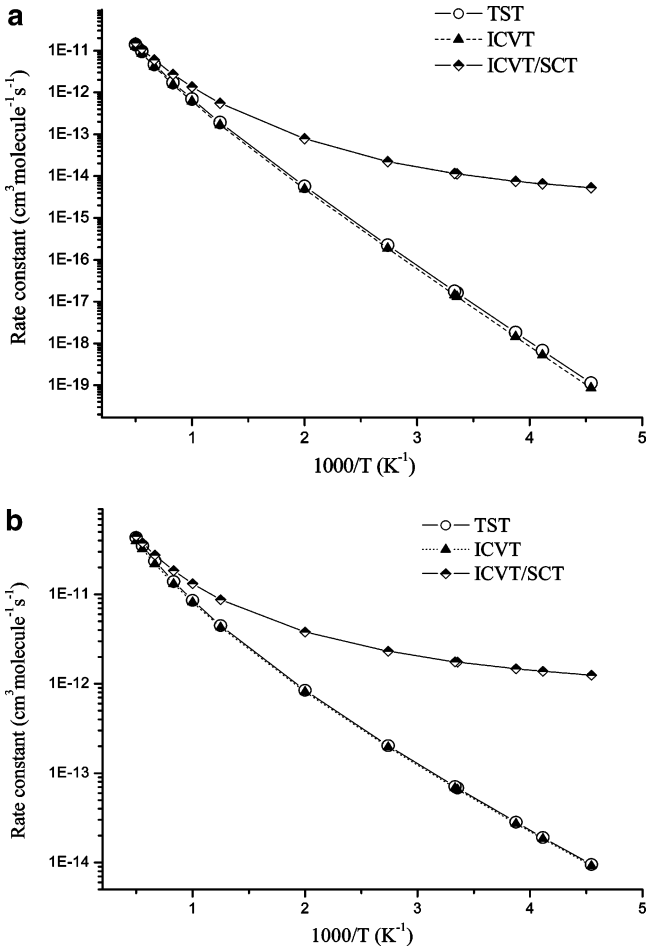

Figure 5. Plot of the TST, ICVT, and ICVT/SCT rate constants (cm^3 molecule^{-1} s^{-1}) calculated at the G3//MP2/6-311+G(2d, 2p) level versus 1000/T between 220 and 2000 K for (a) Cl + HOCl → HCl + Cl and **(b)** Cl + HOCl → Cl_2 + OH.

contamination is much high for the four TSs than for both the reactant and product radicals. For example, the $\langle s^2 \rangle$ values before spin annihilation are 0.78, 0.88, 0.80, and 0.85 for the four TSs, respectively, whereas the $\langle s^2 \rangle$ values never exceed 0.77 for the product radicals. A schematic potential energy surface of both reactions obtained at the MP2/6-311+G(2d, 2p) and G3//MP2 levels with zero-point energy (ZPE) correction is plotted in Figure 2a and b, respectively. Note that the energy of reactant R is set to zero as a reference. For reactions 1a and 1b, the complex (C1 or C2) is first formed, with the relative energy of 2.35 or 1.85 kcal mol^{-1} lower than that of the reactant at the G3//MP2 level; then starting from the complex, the reaction passes through a transition state to form the products. In the case of H + HOCl, the feature of the PES is the direct abstraction mechanism. With respect to the barrier heights, the G3 single-point calculations using the optimized geometries of TSs decrease the calculated results obtained at the MP2/6-311+G(2d, 2p) level by about 7−14 kcal mol^{-1}. Also, it is found that the transition state of Cl abstraction (channel b for each reaction) with a barrier of 1.86 kcal mol^{-1} for R1b and 1.12 kcal mol^{-1} for R2b lies much lower than that of H abstraction, which involves 7.77 and 10.54 kcal mol^{-1} barriers for R1a and R2a, respectively. As a result, the Cl-abstraction pathway will dominate product formation for both reactions. This result shows that the deactivation of the H position and a highly reactive Cl position for Cl abstraction in HOCl is in line with the fact that the bond dissociation energy for H−O (93.93 kcal mol^{-1}) is much higher than that for Cl−O (53.87 kcal mol^{-1}) at the G3//MP2 level.

In addition, we can find that the barrier heights of the reverse reaction (−1b) are 13.12 and 3.95 kcal mol^{-1} at the MP2 and G3//MP2 levels, respectively. The forward reaction (1b) barrier (1.86 kcal mol^{-1}) is less than the reverse reaction (−1b) barrier (3.95 kcal mol^{-1}), so it may be expected that the forward reaction may happen more easily than the reverse reaction.

2. Dynamics Calculations. The MEP for each reaction channel is calculated by IRC theory at the MP2/6-311+G(2d, 2p) level, and the dynamics calculations of the title reactions are carried out with the VTST-ISPE method at the G3//MP2 level. Figure 3 depicts the classical potential energy curve ($V_{MEP}(s)$), the vibrationally adiabatic ground-state potential energy curve ($V_a^G(s)$), and the zero-point energy (ZPE) curve for reaction 1a as a function of the intrinsic reaction coordinate s. Those for the other three reactions are given in Figure S1 of Supporting Information. Note that the maximum of the potential energy profile at the G3//MP2 level is slightly shifted in the s direction in Figure 3. This is the case in which the saddle point position of the dual level is generally shifted with the VTST-ISPE scheme.[20] Similar behavior can be drawn from reactions 1b, 2a, and 2b.

The changes in the generalized normal-mode vibrational frequencies along the MEP for reactions 1a and 1b are shown in Figure 4a and b, and those for reactions 2a and 2b are given in Figure S2 of Supporting Information. In Figure 4a, in the

TABLE 3: Rate Constants (cm^3 $molecule^{-1}$ s^{-1}) for the Reaction HOCl + Cl in the Temperature Range from 220−2000 K[a]

T(K)	k_{1a}	k_{1b}	k_1	exptl
220	5.27×10^{-15}	1.25×10^{-12}	1.26×10^{-12}	
243	6.51×10^{-15}	1.38×10^{-12}	1.39×10^{-12}	$(1.75 \pm 0.2) \times 10^{-12}$ *b*
258	7.52×10^{-15}	1.47×10^{-12}	1.48×10^{-12}	$(1.79 \pm 0.08) \times 10^{-12}$ *b*
298	1.12×10^{-14}	1.75×10^{-12}	1.76×10^{-12}	$(1.4 \pm 0.37) \times 10^{-12}$ *c* $(1.9 \pm 0.3) \times 10^{-12}$ *d* $(2.28 \pm 0.09) \times 10^{-12}$ *e*
300	1.15×10^{-14}	1.76×10^{-12}	1.77×10^{-12}	1.83×10^{-12} [b]
365	2.23×10^{-14}	2.31×10^{-12}	2.33×10^{-12}	$(2.08 \pm 0.16) \times 10^{-12}$ *b*
500	7.80×10^{-14}	3.80×10^{-12}	3.88×10^{-12}	
800	5.56×10^{-13}	8.74×10^{-12}	9.30×10^{-12}	
1000	1.35×10^{-12}	1.32×10^{-11}	1.46×10^{-11}	
1200	2.70×10^{-12}	1.84×10^{-11}	2.11×10^{-11}	
1500	5.99×10^{-12}	2.75×10^{-11}	3.35×10^{-11}	
1800	1.10×10^{-11}	3.77×10^{-11}	4.87×10^{-11}	
2000	1.54×10^{-11}	4.50×10^{-11}	6.04×10^{-11}	

[a] k_{1a} and k_{1b} represent the ICVT/SCT rate constants of reactions R1a and R1b, and k_1 represents the total rate constant calculated from the sum of the two ICVT/SCT rate constants. [b] From ref 3. [c] From ref 4. [d] From ref 5. [e] From ref 6.

reactant region at about $s = -2.0$ $(amu)^{1/2}$ bohr, the frequencies are associated with those of complex C1, and in the positive limit of s ($s = +\infty$), the frequencies correspond to the products HCl and ClO. Most of the frequencies except those for mode 5 do not change significantly on going from the reactants to the products. The frequency curve of mode 5 has the greatest drop in the region from $s = -1.0$ to 1.0 $(amu)^{1/2}$ bohr. This mode connects the frequency of the H−O stretching vibration of HOCl with the frequency of the H−Cl stretching vibration of HCl. Therefore, mode 5 can be referred to as the "reactive mode" in reaction 1a. The three lowest harmonic frequencies are the transitional modes, which correspond to free rotations and translations that evolve into vibration. Similar behavior can be drawn from reactions 1b, 2a, and 2b, although for the Cl-abstraction reaction channels (R1b and R2b) the change in the reactive mode is not as large as that for the H-abstraction channels (R1a and R2a).

The rate constants for each reaction channel are calculated by using the conventional transition-state theory (TST), improved canonical variational transition-state theory (ICVT), and ICVT with the small-curvature tunneling correction (SCT) over the temperature range from 220 to 2000 K at the G3//MP2 level. The total rate constant for each reaction is obtained from the sum of the individual rate constants associated with the two channels.

The TST, ICVT, and ICVT/SCT rate constants of reaction 1 are presented in Figure 5. As can be seen from Figure 5a and b, the rate constants of TST and ICVT are nearly the same over the whole temperature range, which means that the variational effect for reaction 1 is very small or almost negligible. The ICVT/SCT rate constants are much greater than the ICVT rate constants in the range from 220−500 K. For example, the $k_{ICVT/SCT}/k_{ICVT}$ ratios for channel 1a are 799, 16, and 1.4 at 300, 500, and 1500 K, respectively, and the corresponding values of channel 1b are 26, 4.7, and 1.3, respectively. Thus, SCT correction plays an important role for both channels of reaction 1 in the low-temperature range; in particularly, it is more important for H abstraction than for Cl abstraction. Note that the tunneling factor is very sensitive to the particle mass and energy and the barrier height and shape.[27−29] It is reasonable that the tunneling effect is important in reactions involving H transfer (R1a in this paper). Compared with H-abstraction channel 1a, Cl-abstraction channel 1b, which involves all

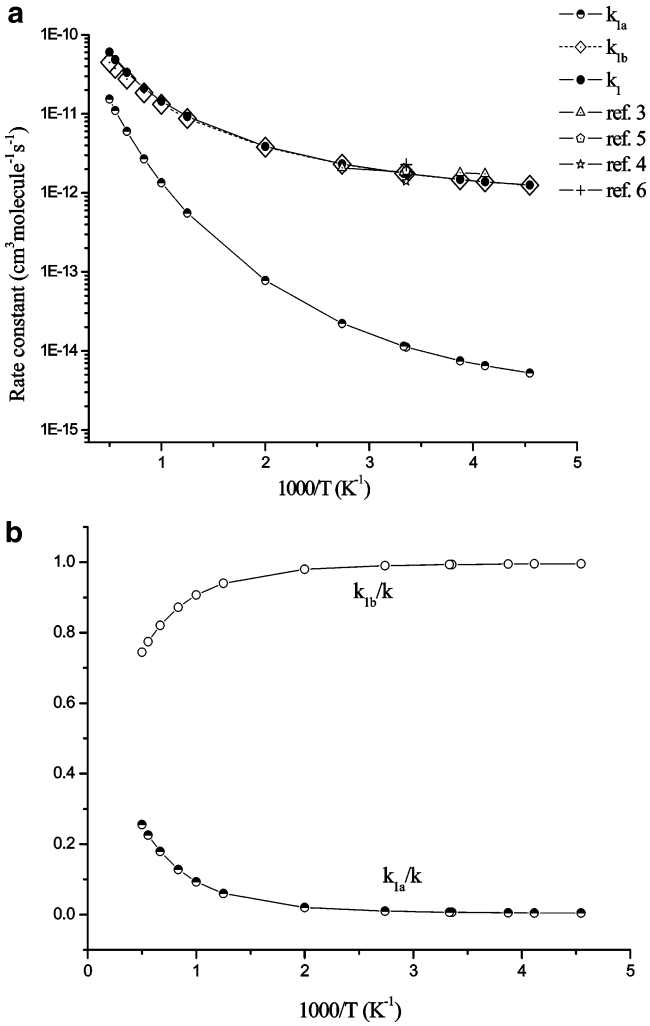

Figure 6. (a) Plot of the calculated individual rate constants k_{1a} and k_{1b}, the total rate constants k_1, and the available experimental values versus 1000/*T* between 220 and 2000 K. (b) Calculated branching ratio versus 1000/*T* between 220 and 2000 K.

"heavies", has a relative lower barrier height (1.86 vs 7.77 kcal mol^{-1}) and a narrower barrier width. (The barrier width at half-height, $\Delta s_{1/2}$, is 1.1 and 0.5 Å for reactions 1a and 1b, respectively.) These factors may result in a greater tunneling contribution in the rate-constant calculation for reaction 1b.

The ICVT/SCT rate constants k_{1a} and k_{1b} and the total rate constant k_1 along with the available experimental values are listed in Table 3. Both theoretical and experimental rate constants are plotted against 1000/*T* (K^{-1}) in Figure 6a, and the temperature dependence of the k_{1a}/k_1 and k_{1b}/k_1 branching ratios is exhibited in Figure 6b. It can be found that the value of k_{1b} is greater than that of k_{1a} by about 1 to 2 orders of magnitude in the low-temperature range from 400−220 K, and the total rate constant is almost equal to that of reaction 1b. The calculated branching ratio k_{1b}/k_1, which is 99% at 298 K, shows good consistency with the result of Ennis et al.[5] (0.91 ± 0.06) and Kukui et al.[6] (0.96 ± 0.05) within experimental uncertainty but is in great disagreement with (0.24 ± 0.11) given by Vogt et al.[4] Thus, on the basis of our calculations, the major reaction channel of Cl + HOCl is chloride abstraction to yield products OH + Cl_2 rather than hydrogen abstraction at lower temperatures. However, as shown in Figure 6b, the contribution from hydrogen abstraction leading to HCl + ClO as a minor product channel increases with the increase in the temperature. For example, the k_{1a}/k_1 ratio is about 2% at 500 K, 18% at 1500

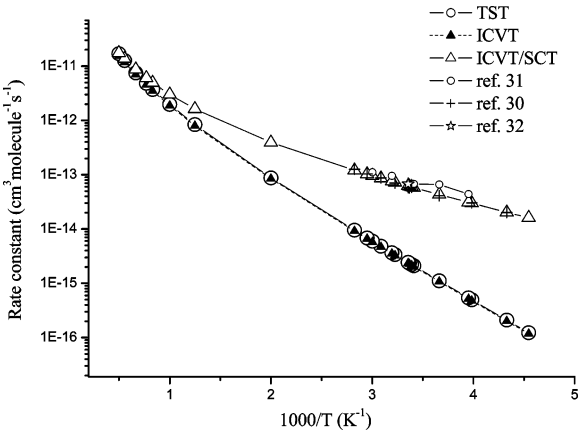

Figure 7. Plot of the TST, ICVT, ICVT/SCT, and the available experimental values versus 1000/T between 220 and 2000 K for $Cl_2 + OH \rightarrow HOCl + Cl$.

TABLE 4: Rate Constants (cm^{3}Molecule^{-1}s^{-1}) for the Reaction $Cl_2 + OH \rightarrow HOCl + Cl$ over the Temperature Range 220−2000 K

T(K)	TST	ICVT	ICVT/SCT	exptl
220	1.23×10^{-16}	1.18×10^{-16}	1.61×10^{-14}	
231	2.10×10^{-16}	2.02×10^{-16}	2.04×10^{-14}	$(2.01 \pm 0.14) \times 10^{-14}$*a*
251	4.97×10^{-16}	4.79×10^{-16}	2.99×10^{-14}	$(3.02 \pm 0.17) \times 10^{-14}$*a*
253	5.37×10^{-16}	5.18×10^{-16}	3.10×10^{-14}	$(4.4 \pm 0.4) \times 10^{-14}$*b*
273	1.11×10^{-15}	1.07×10^{-15}	4.31×10^{-14}	$(4.12 \pm 0.10) \times 10^{-14}$*a*
				$(6.6 \pm 1.4) \times 10^{-14}$*b*
293	2.09×10^{-15}	2.02×10^{-15}	5.79×10^{-14}	$(6.8 \pm 1.0) \times 10^{-14}$*b*
295	2.22×10^{-15}	2.14×10^{-15}	5.96×10^{-14}	$(5.85 \pm 0.30) \times 10^{-14}$*a*
297	2.35×10^{-15}	2.27×10^{-15}	6.12×10^{-14}	$(5.74 \pm 0.43) \times 10^{-14}$*a*
298	2.42×10^{-15}	2.34×10^{-15}	6.20×10^{-14}	$(5.76 \pm 0.63) \times 10^{-14}$*a*
				$(6.70 \pm 0.72) \times 10^{-14}$*c*
310	3.37×10^{-15}	3.26×10^{-15}	7.27×10^{-14}	$(7.00 \pm 0.31) \times 10^{-14}$*a*
313	3.65×10^{-15}	3.53×10^{-15}	7.55×10^{-14}	$(9.5 \pm 1.0) \times 10^{-14}$*b*
324	4.82×10^{-15}	4.66×10^{-15}	8.63×10^{-14}	$(8.72 \pm 0.22) \times 10^{-14}$*a*
333	5.98×10^{-15}	5.78×10^{-15}	9.59×10^{-14}	$(11.1 \pm 2.6) \times 10^{-14}$*b*
339	6.86×10^{-15}	6.63×10^{-15}	1.03×10^{-13}	$(10.3 \pm 0.64) \times 10^{-14}$*a*
354	9.49×10^{-15}	9.18×10^{-15}	1.21×10^{-13}	$(12.6 \pm 0.84) \times 10^{-14}$*a*
500	8.75×10^{-14}	8.44×10^{-14}	3.94×10^{-13}	
800	8.34×10^{-13}	7.98×10^{-13}	1.63×10^{-12}	
1000	1.98×10^{-12}	1.88×10^{-12}	3.03×10^{-12}	
1200	3.72×10^{-12}	3.50×10^{-12}	4.94×10^{-12}	
1500	7.50×10^{-12}	6.99×10^{-12}	8.76×10^{-12}	
1800	1.27×10^{-11}	1.17×10^{-11}	1.37×10^{-11}	
2000	1.69×10^{-11}	1.54×10^{-11}	1.76×10^{-11}	

[a] From ref 30. [b] From ref 31. [c] From ref 32.

K, and 25% at 2000 K. Consequently, two abstraction pathways (i.e., Cl abstraction and H abstraction) will contribute to the whole reaction rate at high temperature. The calculated rate constants of reaction R1 are in excellent agreement with the available experimental values in the measured temperature range from 243−365 K.[3−6] The deviation between the theoretical and experimental values remains within a factor of approximately 0.8 to 1.3. Moreover, the Arrhenius expression of $k_1 = 6.29 \times 10^{-12} \exp(-372/T)$ cm^3 molecule^{-1} s^{-1} fitted by the ICVT/SCT rate constant in the temperature range from 243−365 K is in good accord with that reported by Cook et al.,[3] $k = (3.0 \pm 0.5) \times 10^{-12} \exp[-(130 \pm 60)/T]$ cm^3 molecule^{-1} s^{-1}. The three-parameter expressions using the ICVT/SCT rate constants in the 220−2000 K range for H and Cl abstraction are $k_{1a} = 5.89 \times 10^{-25} T^{4.07} \exp(169.8/T)$ and $k_{1b} = 1.02 \times 10^{-17} T^{2.01} \exp(192.6/T)$ cm^3 molecule^{-1} s^{-1}.

Figure 7 presents the rate constants of the reverse reaction $OH + Cl_2 \rightarrow Cl + HOCl$. The calculated rate constants and the corresponding experimental values[30−32] are listed in Table 4. The deviation factor between theoretical and the experimental

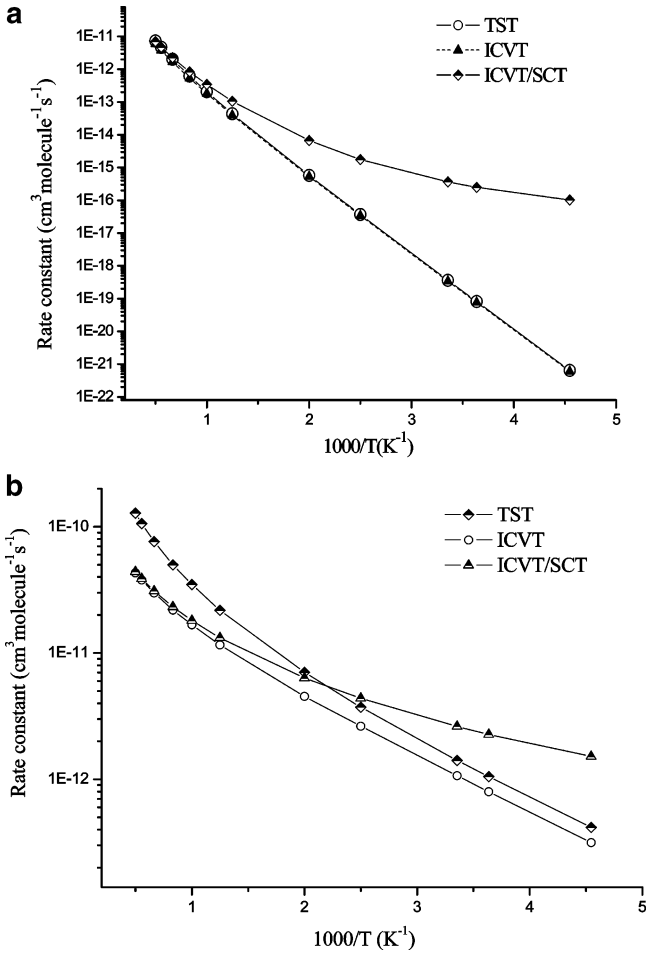

Figure 8. Plot of the TST, ICVT, and ICVT/SCT rate constants (cm^3 molecule^{-1} s^{-1}) calculated at the G3//MP2/6-311+G(2d, 2p) level versus 1000/T between 220 and 2000 K for (a) $H + HOCl \rightarrow H_2 + ClO$ and (b) $H + HOCl \rightarrow HCl + OH$.

rate constants is approximately 0.9 to 1.5 in the temperature range from 231−354 K. The calculated activation energies are 2.35 and 2.37 kcal mol^{-1}, in reasonable agreement with the corresponding experimental values of 2.44 and 1.81 kcal mol^{-1} in the temperature ranges from 231−354[30] and 253−333 K,[31] respectively. Seen from Tables 3 and 4, the rate constant of the reverse reaction is much lower than that of forward reaction 1b because of a higher potential barrier.

As shown from Figure 8a and b, where the rate constants of TST, ICVT, and ICVT/SCT for reactions 2a and 2b are plotted, respectively, the difference between the TST and ICVT rate constants implies that the variational effect is very small for channel 2a, whereas it becomes important for channel 2b. The $k_{ICVT/SCT}/k_{ICVT}$ ratios are 1067 and 2.4 at 298 K, 13 and 1.4 at 500 K, and 1.3 and 1.0 at 1500 K for R2a and R2b, respectively, indicative of much more significant SCT correction in the low-temperature range on calculations of the rate constants for H abstraction than for Cl abstraction, which is similar to the reaction of HOCl with Cl. The ICVT/SCT rate constants for each reaction channel and the total rate constant k_2 are presented in Table 5 and in Figure 9a. The branching ratios of k_{2a}/k_2 and k_{2b}/k_2 are plotted in Figure 9b. It is seen that the calculated rate constant k_2 agrees well with the experimental values[4,7] at 298 K. The branching ratio to channel 2b ranges from more than 99% at 298 K to 86% at 2000 K. The theoretical results suggest that the reaction of HOCl with H atoms proceeds predominantly via Cl abstraction over the whole temperature range. The three-parameter expressions fitted by the ICVT/SCT rate constants

TABLE 5: Rate Constants (cm^3 $molecule^{-1}$ s^{-1}) for the Reaction HOCl + H in the Temperature Range from 220−1500 K[a]

T(K)	k_{2a}	k_{2b}	k_2	exptl
220	1.03×10^{-16}	1.52×10^{-12}	1.52×10^{-12}	
275	2.50×10^{-16}	2.26×10^{-12}	2.26×10^{-12}	
298	3.64×10^{-16}	2.62×10^{-12}	2.62×10^{-12}	$(3.5 \pm 0.7) \times 10^{-12}$[b] $(5.0 \pm 1.4) \times 10^{-12}$[c]
400	1.77×10^{-15}	4.39×10^{-12}	4.39×10^{-12}	
500	6.70×10^{-15}	6.34×10^{-12}	6.35×10^{-12}	
800	1.05×10^{-13}	1.32×10^{-11}	1.33×10^{-11}	
1000	3.43×10^{-13}	1.81×10^{-11}	1.84×10^{-11}	
1200	8.31×10^{-13}	2.32×10^{-11}	2.40×10^{-11}	
1500	2.24×10^{-12}	3.10×10^{-11}	3.32×10^{-11}	
1800	4.69×10^{-12}	3.88×10^{-11}	4.35×10^{-11}	
2000	6.99×10^{-12}	4.40×10^{-11}	5.10×10^{-11}	

[a] k_{2a} and k_{2b} represent the ICVT/SCT rate constants of reactions 2a and 2b, respectively, and k_2 represents total rate constant calculated from the sum of the two ICVT/SCT rate constants. [b] From ref 4. [c] From ref 7.

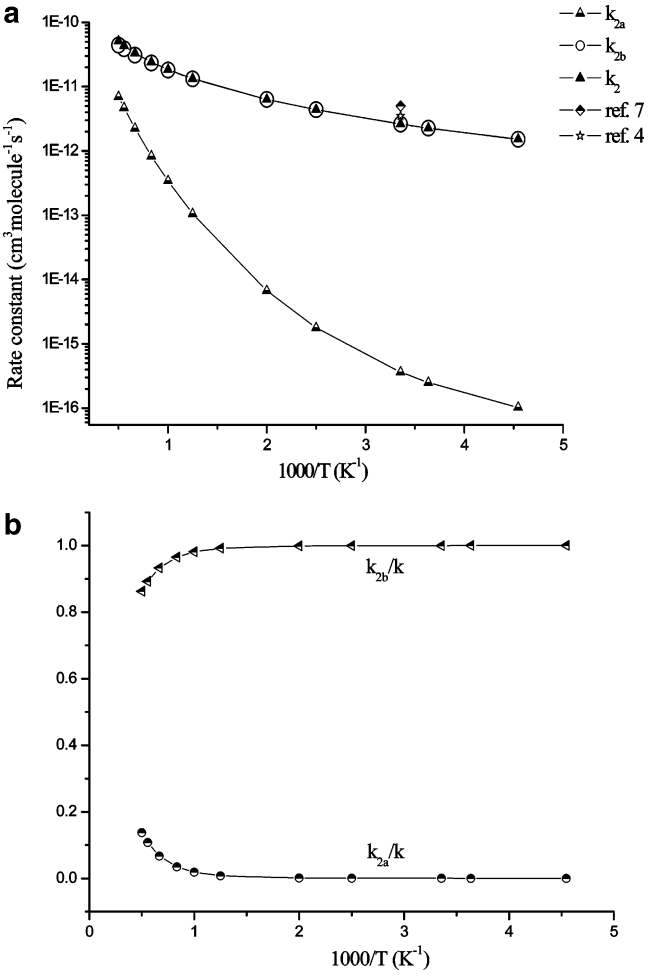

Figure 9. (a) Plot of the calculated individual rate constants k_{2a} and k_{2b}, the total rate constants k_2, and the available experimental values versus 1000/T between 220 and 2000 K. (b) Calculated branching ratio versus 1000/T between 220 and 2000 K.

are $k_{2a} = 7.31 \times 10^{-28}T^{4.89}$ exp(−214.1/T) and $k_{2b} = 5.27 \times 10^{-15}T^{1.20}$ exp(−187.3/T) cm^3 $molecule^{-1}$ s^{-1} for the two channels of reaction R2, respectively, in the range from 220−2000 K.

Owing to the good agreement between the theoretical and experimental values, it is reasonable to believe that our calculated results will provide a good estimate for the kinetics of the reactions in the high-temperature range. Therefore, for the convenience of future experimental measurements, the three-parameter fits for the ICVT/SCT rate constants for the title reactions as well as the reverse reaction of R1b within 220−2000 K give the following expressions (in cm^3 $molecule^{-1}$ s^{-1}):

$$k_1 = 1.29 \times 10^{-18}T^{2.31} \exp(295.3/T)$$

$$k_2 = 1.61 \times 10^{-15}T^{1.37} \exp(-121.3/T)$$

$$k_{-1b} = 2.68 \times 10^{-18}T^{2.10} \exp(-577.0/T)$$

Conclusions

In this paper, we employ an ab initio direct dynamic method to study the reactions of Cl + HOCl and H + HOCl, for which two kinds of reaction mechanisms are presented by experiments (i.e., the abstraction of the hydrogen or the chloride as the major reaction channel). Dynamics calculations are carried out using variational transition-state theory with the interpolated single-point energy method (VTST-ISPE) at the G3//MP2/6-311+G(2d, 2p) level. The calculated rate constants of the two reactions and the reverse reaction of R1b by the improved canonical variational transition-state theory (ICVT) with a small-curvature tunneling correction (SCT) are in good agreement with the available experimental values. The reaction Cl + HOCl proceeds via a complex and then a transition state, and the H + HOCl reaction proceeds as a direct H- or Cl-abstraction reaction without an intermediate complex. It is shown that for the Cl + HOCl reaction, chlorine abstraction giving Cl_2 + OH as products prevails at low temperatures, and products HCl + ClO occupy only a small part in the high-temperature range. In the case of the reaction H + HOCl, the chlorine-abstraction pathway to yield the products HCl + OH dominates the reaction over the whole temperature range. The three-parameter expressions (in cm^3 $molecule^{-1}$ s^{-1}) for two reactions within 220−2000 K are $k_1 = 1.29 \times 10^{-18}T^{2.31}$ exp(295.3/T) and $k_2 = 1.61 \times 10^{-15}$ $T^{1.37}$ exp(−121.3/T). We hope that the theoretical results may be useful for estimating the kinetics of the reactions over a wide temperature range where no experimental data is available.

Acknowledgment. We thank Professor Donald G. Truhlar for providing the POLYRATE 8.4.1 program. This work was supported by the National Natural Science Foundation of China (20073014), the Doctor Foundation by the Ministry of Education, the Foundation for University Key Teacher by the Ministry of Education, the Key Subject of Science and Technology by the Ministry of Education of China, and the Innovational Foundation by Jilin University.

Supporting Information Available: Potential energy, ground-state vibrationally adiabatic, and zero-point energy curves as functions of s(amu)$^{1/2}$ bohr. Changes in the generalized normal-mode vibrational frequencies as a function of s(amu)$^{1/2}$ bohr. This material is available free of charge via the Internet at http://pubs.acs.org.

References and Notes

(1) *Scientific Assessment of Ozone Depletion, 1994*; WMO Global Ozone Research Monitoring Project, Report 37, 1995.

(2) Prasad, S. S. *Plant. Space Sci.* **1976**, *24*, 1187.

(3) Cook, J. L.; Ennis, C. A.; Leck, T. J.; Birks, J. W. *J. Chem. Phys.* **1981**, *74*, 545.

(4) Vogt, R.; Schindler, R. N. *Ber. Bunsen-Ges. Phys. Chem.* **1993**, *97*, 819.

(5) Enis, C. A.; Birks, J. W. *J. Phys. Chem.* **1985**, *89*, 186.

(6) Kukui, A.; Roggenbuck, J.; Schindler, R. N.; *Ber. Bunsen-Ges. Phys. Chem.* **1997**, *101*, 281.
(7) Ennis, C. A.; Birks, J. W. *J. Phys. Chem.* **1988**, *92*, 1119.
(8) Truhlar, D. G. In *The Reaction Path in Chemistry: Current Approaches and Perspectives*; Heidrich, D., Ed.; Kluwer: Dordrecht, The Netherlands, 1995; p 229.
(9) Truhlar, D. G.; Garrent, B. C.; Klippenstein, S. J. *J. Phys. Chem.* **1996**, *100*, 12771.
(10) Hu, W. P.; Truhlar, D. G. *J. Am. Chem. Soc.* **1996**, *118*, 860.
(11) Chuang, Y.-Y.; Corchado, J. C.; Fast, P. L.; Villa, J.; Hu, W.-P.; liu, Y.-P.; Lynch, G. C.; Jackels, C. F.; Nguyen, K. A.; Gu, M. Z.; Rossi, I.; Coitino, E. L.; Clayton, S.; Melissas, V. S.; Lynch, B. J.; Steckler, R.; Garrett, B. C.; Isaacson, A. D.; Truhlar, D. G. *Polyrate*, version 8.4.1; University of Minnnesota: Minneapolis, MN, 2000.
(12) Truhlar, D. G.; Garrett, B. C. *Acc. Chem. Res.* **1980**, *13*, 440.
(13) Truhlar, D. G.; Isaacson, A. D.; Garrett, B. C. In *The Theory of Chemical Reaction Dynamics*; Baer, M., Ed.; CRC Press: Boca Raton, FL, 1985; p 65.
(14) Truhlar, D. G.; Garrett, B. C. *Annu. Rev. Phys. Chem.* **1984**, *35*, 159.
(15) Garrett, B. C.; Truhlar, D. G.; Grev, R. S.; Magnuson, A. W. *J. Phys. Chem.* **1980**, *84*, 1730.
(16) Lu, D. H.; Truong, T. N.; Melissas, V. S.; Lynch, G. C.; liu, Y. P.; Grarrett, B. C.; Steckler, R.; Issacson, A. D.; Rai, S. N.; Hancock, G. C.; Lauderdale, J. G.; Joseph, T.; Truhlar, D. G. *Comput. Phys. Commun.* **1992**, *71*, 235.
(17) Liu, Y.-P.; Lynch, G. C.; Truong, T. N.; Lu, D.-h.; Truhlar, D. G.; Garrett, B. C. *J. Am. Chem. Soc.* **1993**, *115*, 2408.
(18) Frisch, M. J.; Trucks, G. W.; Schlegel, H. B.; Scuseria, G. E.; Robb, M. A.; Cheeseman, J. R.; Zakrzewski, V. G.; Montgomery, J. A., Jr.; Stratmann, R. E.; Burant, J. C.; Dapprich, S.; Millam, J. M.; Daniels, A. D.; Kudin, K. N.; Strain, M. C.; Farkas, O.; Tomasi, J.; Barone, V.; Cossi, M.; Cammi, R.; Mennucci, B.; Pomelli, C.; Adamo, C.; Clifford, S.; Ochterski, J.; Petersson, G. A.; Ayala, P. Y.; Cui, Q.; Morokuma, K.; Malick, D. K.; Rabuck, A. D.; Raghavachari, K.; Foresman, J. B.; Cioslowski, J.; Ortiz, J. V.; Stefanov, B. B.; Liu, G.; Liashenko, A.; Piskorz, P.; Komaromi, I.; Gomperts, R.; Martin, R. L.; Fox, D. J.; Keith, T.; Al-Laham, M. A.; Peng, C. Y.; Nanayakkara, A.; Gonzalez, C.; Challacombe, M.; Gill, P. M. W.; Johnson, B. G.; Chen, W.; Wong, M. W.; Andres, J. L.; Head-Gordon, M.; Replogle, E. S.; Pople, J. A. *Gaussian 98*, revision X; Gaussian, Inc.: Pittsburgh, PA, 1998.
(19) Curtiss, L. A.; Raghavachari, K.; Redfern, P. C.; Rassolov, V.; Pople, J. A. *J. Chem. Phys.* **1998**, *109*, 7764.
(20) Chuang, Y. Y.; Corchado, J. C.; Truhlar, D. G. *J. Phys. Chem.* **1999**, *103*, 1140.
(21) Truhlar, D. G. *J. Comput. Chem.* **1991**, *12*, 266.
(22) Chuang, Y. Y.; Truhlar, D. G. *J. Chem. Phys.* **2000**, *112*, 1221.
(23) Kuchitsu, K. In *Structure of Free Polyatomic Molecules: Basic Data*; Springer: Berlin, 1998; Vol. 1, p 35.
(24) Distelrath, V.; Boesl, U. *Faraday Discuss. Chem. Soc.* **2000**, *115*, 161.
(25) Chase, M. W., Jr. *J. Phys. Chem. Ref. Data* **1998**, Monograph 9, 1−1951 (NIST-JANAF Themochemical Tables, 4th ed.).
(26) Junttila, M.-L.; Lafferty, W. J.; Burkholder, J. B. *J. Mol. Spectrosc.* **1994**, *164*, 583.
(27) Stern, M. J.; Weston, R. E. *J. Chem. Phys.* **1974**, *60*, 2803.
(28) Stern, M. J.; Weston, R. E. *J. Chem. Phys.* **1974**, *60*, 2808.
(29) Stern, M. J.; Weston, R. E. *J. Chem. Phys.* **1974**, *60*, 2815.
(30) Gilles, M. K.; Burkholder, J. B.; Ravishankara, A. R. *Int. J. Chem. Kinet.* **1999**, *31*, 417.
(31) Boodaghians, R. B.; Hall, I. W.; Wayne, R. P. *J. Chem. Soc., Faraday Trans.* **1987**, *83*, 529.
(32) Loewenstein, L. M.; Anderson, J. G. *J. Phys. Chem.* **1984**, *88*, 6277.